

Coronary Angiography

Noninvasive Assessment of Myocardial Stunning from Short-Term Coronary Occlusion Using Tagged Magnetic Resonance Imaging

Dara L. Kraitchman,¹ Hanns B. Hillenbrand,¹ Izlem Oznur,¹ Joao A.C. Lima,^{1,2} Elliot R. McVeigh,¹ Elias A. Zerhouni,¹ and David A. Bluemke¹

¹Department of Radiology, Johns Hopkins University, Baltimore, Maryland

²Department of Cardiology, Johns Hopkins University, Baltimore, Maryland

ABSTRACT

Brief myocardial ischemia of less than 20 min duration, followed by reperfusion, is known to cause transient contractile dysfunction, often termed myocardial stunning. Tagged magnetic resonance imaging offers a noninvasive method that can be used to quantify this regional mechanical dysfunction in stunned myocardium. To this end, a closed-chest canine model of myocardial stunning was created by short-term (~20-min) coronary occlusion, via inflation of an angioplasty balloon placed fluoroscopically in the left anterior descending (LAD) coronary, followed by reperfusion. Changes in myocardial strain before occlusion, during occlusion, and at 15 and 30 min after reperfusion were determined using repeated-measures analysis of variance. After instrumentation but before coronary occlusion, global reductions in myocardial strain were observed relative to animals that did not undergo coronary catheterization procedures. Declines of 46% and 49% in regional myocardial blood flow in the LAD and left circumflex bed, respectively, from preinstrumentation levels occurred due to coronary angiography and placement of a deflated angioplasty balloon in the LAD for 1 hr. During LAD occlusion, maximum myocardial shortening was significantly reduced in the anterior and antero-septal regions of the left ventricular apex (i.e., ischemic region) but returned to baseline values by 30 min after reperfusion. No augmentation of myocardial function was observed in the nonischemic regions during occlusion or reperfusion. Thus, this noninvasive technique to evaluate myocardial ischemia demonstrated a graded response in myocardial function to ischemia and persistent regional dysfunction or “myocardial stunning” after short-term coronary occlusion.

KEY WORDS: MR tagging; Myocardial function; Myocardial ischemia; Myocardial stunning.

Received January 29, 1999; Accepted October 28, 1999

Address reprint requests to Dara L. Kraitchman.

INTRODUCTION

Brief myocardial ischemia of less than 20 min duration, followed by reperfusion, is known to cause transient contractile dysfunction (1–3), often termed myocardial stunning (4). Understanding the time course of functional recovery and the ability to differentiate reversible and nonreversible dysfunction are important for serial patient assessment. Thus, many animal models have been developed to study myocardial stunning in detail (3,5–7).

However, observations in animal models of myocardial stunning are often confounded by the effects of the invasive techniques. For example, open-chest surgery, which is used to create coronary occlusion, may alter regional myocardial function (8). In addition, the implantation of ultrasonic crystals or beads, to create material points for tracking of regional myocardial motion, may damage the myocardium and disturb normal cardiac mechanics (8). Magnetic resonance imaging (MRI) offers a noninvasive quantitative method to study regional functional changes after myocardial stunning. In the first MRI evaluation to characterize the relationship between perfusion and function in stunned myocardium, an open-chest animal model was used to assess wall thickening (9). Aside from possible mechanical alterations caused by open-chest surgery, wall thickening was evaluated only in a single imaging slice, and differences in function across the wall (e.g., endocardial vs. epicardial) were not assessed in this study.

Thus, the purpose of this study was to assess quantitatively the recovery of regional myocardial function using MRI tissue tagging (10,11) over the entire left ventricle in a closed-chest animal model of myocardial stunning produced by short-term coronary occlusion. Coronary occlusion was created in a closed-chest manner using balloon angioplasty techniques. This animal model of closed-chest coronary occlusion has been used previously to create experimental myocardial infarction for MRI determination of myocardial function (12) and myocardial perfusion patterns (13). However, this closed-chest model of coronary occlusion to create myocardial dysfunction without loss of viability (i.e., no myocardial infarction) to study the mechanics of myocardial stunning has not been reported previously.

Because the effect of coronary catheterization and angioplasty balloon placement on myocardial function has not been quantified previously by MRI, we compared baseline function after instrumentation (but before coronary occlusion) to function in anesthetized animals that did not undergo coronary catheterization (which were previously studied [14]). We hypothesized that our base-

line motion studies with a deflated angioplasty balloon in the left anterior descending (LAD) placed before MRI would not cause significant functional alterations, because noncritical coronary stenoses that reduce blood flow by only 20–50% are not expected to result in functional abnormalities at rest. Regional myocardial function during coronary occlusion and after reperfusion were determined with tagged MRI. Thus, using MRI as a high-resolution method for studying regional function, we report the effects of instrumentation, wall motion changes associated with brief coronary occlusion, and the time course of myocardial stunning after reperfusion.

MATERIALS AND METHODS

Experimental Preparation

All animal studies were approved by the Institutional Animal Care and Use Committee and adhered to the American Veterinary Medical Association guidelines. Eight mongrel dogs (20–25 kg) underwent coronary angiography and angioplasty balloon catheter placement for a short-term (<20-min) acute occlusion followed by reperfusion to generate myocardial stunning. All animals were preanesthetized with 5 mg/kg ketamine, 2.5 mg/kg xylazine, and 0.05 mg/kg atropine. The animals were induced with sodium pentothal and intubated. General anesthesia was maintained with 1–2% isoflurane and mechanical ventilation. A right femoral artery cutdown was performed, and a 6-French pigtail catheter (Cordis, Diamond Bar, CA) was guided under fluoroscopy into the left ventricle for fluorescent microspheres (Dyetrak, Triton Technologies, San Diego, CA) injection to determine regional myocardial blood flow (RMBF). A carotid artery cutdown was also performed and an introducer was placed.

A 7-French right Judkins catheter guided from the carotid artery was used to engage the left main coronary artery after which a 0.014-inch guidewire and an angioplasty balloon catheter were placed in the proximal LAD coronary artery. The guiding catheter was removed from the left main coronary artery without disturbing the guidewire or angioplasty balloon. The animal was transported to the MRI suite for imaging. The guidewire was removed before imaging while leaving the deflated angioplasty balloon in place in the LAD.

Imaging Protocol

All imaging was performed on a 1.5-T MRI scanner (General Electric Medical Systems, Milwaukee, WI).

The animal was imaged under general inhalational anesthesia with mechanical ventilation and placed supine with a surface coil over the heart.

The location and extent of the left ventricle was determined by axial scout images using a segmented k-space, fast spoiled gradient echo pulse sequence (TE 1.2 msec, TR 3.2 msec, field of view 26–28 cm, 10 mm slice thickness, 32 k-space lines per view, and 128×256 image matrix interpolated to 256×256). Images were gated to the QRS complex of the electrocardiogram.

Baseline Function

A three-dimensional (3D) tagged imaging set (i.e., short- and long-axis tagged images) was obtained after instrumentation but before occlusion (by balloon inflation). Tagging enables the creation of noninvasive magnetic markers that are embedded in the myocardium at a specific time point, such as end-diastole (10,15). The markers move as the heart contracts and can be tracked to determine the deformation of the heart. The baseline tagged image set was obtained approximately 1 hr after coronary catheterization was performed.

Short-axis image slices were obtained with parallel tissue tags in two orientations (0- and 90-degree tags; Fig. 1) from end-diastole to end-systole using an electrocardiogram gated, segmented k-space, breathhold, fast, spoiled gradient echo pulse sequence (TE 1.2 msec, TR 3.2 msec, field of view 26–28 cm, 7 mm slice thickness, 0–2 mm gap between slices, 6-pixel tag-to-tag spacing, $104\text{--}110 \times 256$ image matrix interpolated to 256×256 , and flip angle 12 degrees). The segmentation of k-space for each dog was chosen based on heart rate to freeze cardiac motion; in this group of dogs, the number of k-space lines per view varied from 7 to 13 between animals. This resulted in an image acquisition window of 22.4–41.6 msec per cardiac phase (e.g., seven k-space lines per view \times 3.2 msec TR = 22.4 msec). The total number of phase encodes per image (104–110) was taken as a whole multiple of the k-space lines per view (e.g., 13 k-space lines per view \times 8 RR intervals = 104 phase encodes). One short-axis slice location was acquired per breathhold. The two tag orientations (0- and 90-degree parallel tags) were obtained in the same breathhold for each imaging slice. Thus, each breathhold lasted between 16 and 30 heartbeats. Approximately four to seven short-axis slices with five to seven cardiac phases were obtained in each animal.

Six multiphase long-axis images slices with parallel tissue tags in a single orientation (orthogonal to the long axis of the left ventricle; Fig. 1) were acquired using iden-

tical imaging parameters to the short-axis images. The center of the left ventricle in the short axis taken below the mitral valve was used as the pivot point for rotating long-axis slices spaced at 30-degree angular increments. Two long-axis image slice locations were obtained per breathhold. Breathhold in the anesthetized animals was achieved by suspending the ventilator at end-expiration. The ventilator was turned on for approximately 30–45 sec between breathholds. Thus, the entire 3D tagged imaging set was acquired in 15 min.

Occlusion Function

The angioplasty balloon was then inflated. A 3D tagged imaging set was obtained during the next 15 min in the same slice locations as the baseline scan. Fluorescent microspheres were injected into the left ventricle, and a reference blood sample was obtained from the femoral introducer sheath to determine RMBF during occlusion. The balloon was then deflated after 20 min of occlusion.

Early and Late Reperfusion Function

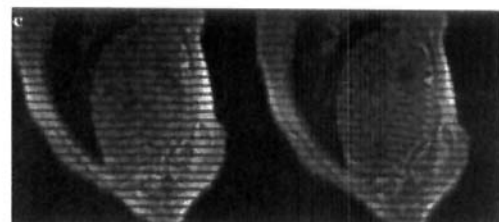
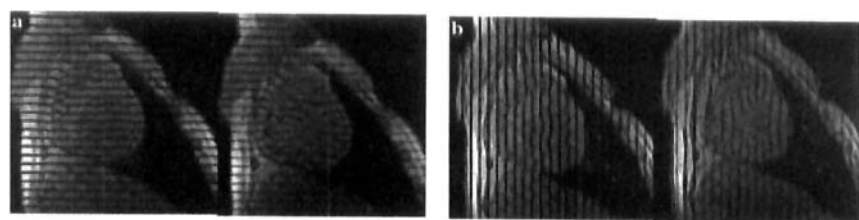
A 3D tagged imaging set was obtained during “early reperfusion” (starting 15 min after reperfusion). Again, the entire 3D tagged imaging set was acquired in 15 min. Therefore, myocardial function determined during early reperfusion was 15–30 min after initiation of reperfusion. After completion of the early reperfusion tagged imaging set, another 3D tagged imaging set was obtained during “late reperfusion” (starting approximately 30 min after reperfusion and finishing at approximately 45 min after reperfusion). A second injection of fluorescent microspheres was then performed, and a reference blood sample was obtained from the femoral introducer sheath to confirm that coronary reperfusion had occurred.

Postmortem Procedures

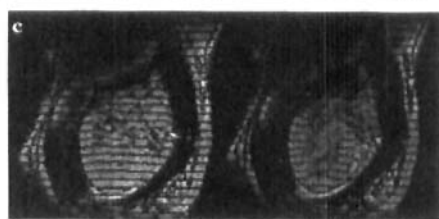
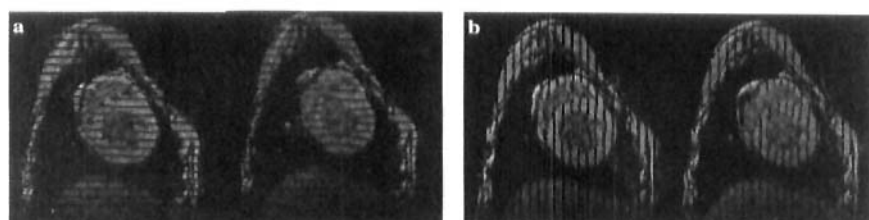
After humane euthanasia, the heart was excised and sliced along the short-axis imaging planes. The heart was incubated in triphenyltetrazolium chloride (TTC) at 38°C to determine myocardial viability. The heart was then photographed. Myocardial samples of each heart slice were then obtained, weighed, and processed along with reference blood samples to determine RMBF by Interactive Medical Technology (North Hollywood, CA).

Radiolabeled Microsphere Measurements

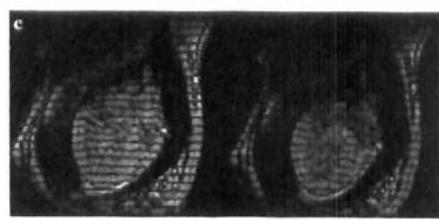
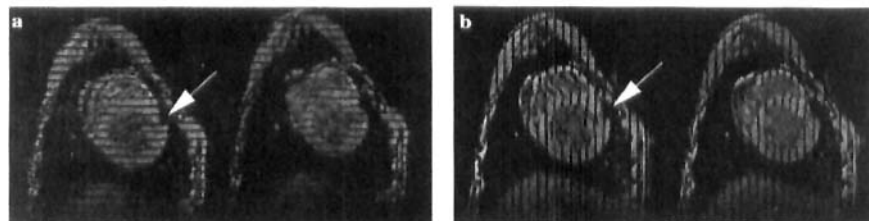
To determine the effect of LAD balloon placement, three mongrel dogs were instrumented in a manner iden-



A. Normal



B. Baseline



C. Occlusion

tical to the eight dogs studied with MRI. Three to five million radiolabeled microspheres (^{153}Gd , ^{46}Sc , ^{113}Sn) were injected into the left ventricle, whereas a reference sample was obtained from the femoral sheath for RMBF measurements at three specific time points: before coronary catheterization, 1 hr after placement of a deflated angioplasty balloon in the LAD, and 15 min after LAD coronary occlusion. The second time point (~1 hr after placement of deflated balloon) represents the approximate time when the baseline tagged MR images were obtained in the eight dogs studied with MRI.

The animal was then humanely euthanized and the heart excised and sliced along the short axis in 10-mm-thick slices. The slices were then photographed. The myocardium was divided into approximately 1-g wedges that were subdivided into three transmural pieces. These pieces were weighed and counted in a gamma counter (HP Model 5986) along with the reference blood samples. RMBF was determined using standard techniques (16).

Data Analysis

The tag lines were detected and tracked on the short- and long-axis images using a custom analysis package (FINDTAGS) (17) running on a Silicon Graphics workstation (SGI, Mountain View, CA). The principal strains were calculated using the two tag orientations obtained in the short-axis images. The left ventricle was divided into five longitudinal regions (base, mid1, mid2, apex1, and apex2), six circumferential regions (anteroseptal, anterior, lateral, posterior, posteroseptal, and septal), and three transmural regions (endocardial, midwall, and epicardial). Maximum principal strain (or greatest shortening), circumferential normal strain (or maximum circumferential shortening), and radial normal strain (or radial thickening) were determined in each of these 90 regions.

To determine whether the presence of a deflated balloon catheter altered regional strain patterns, a comparison was made between the baseline imaging strains and the regional strains in 10 anesthetized normal dogs previously reported (14). These 10 dogs (14), henceforth re-

ferred to as *normal dogs*, had an identical anesthetic protocol to the dogs studied at baseline, occlusion, and reperfusion. The instrumentation of the normal dogs consisted of carotid artery and jugular vein cutdowns for placement, under fluoroscopic guidance, of pressure transducers in the left and right ventricle, respectively. No coronary catheterization was performed in these normal dogs.

Regional strain values in these normal animals were reported previously in 12 anatomic regions (three longitudinal regions—base, midventricle, and apex—and four circumferential regions—septal, anterior, lateral, and posterior) (14). The strains from the baseline imaging in the present study were averaged into these same 12 anatomic regions. Statistically significant differences in strain by longitudinal and circumferential location between normal dogs and baseline imaging were determined using a multivariate analysis of variance (ANOVA). When the effects were significant, post-hoc testing using Scheffé subtesting was performed to determine which longitudinal region (i.e., base, midventricle, and apex) and/or circumferential region (i.e., septal, anterior, lateral, and posterior) contributed to the significant effect. $p < 0.05$ was considered statistically significant.

Statistically significant alterations in regional maximum principal strain, circumferential strain, and radial strain from baseline imaging to occlusion were determined using a repeated-measures ANOVA with Scheffé subtesting. Recovery of function after reperfusion was determined by comparing the early reperfusion strains (i.e., strains at 15 min of reperfusion) to the baseline strains and the late reperfusion strains (i.e., strains at 30 min of reperfusion) to the baseline strains using an ANOVA with Scheffé subtesting. All results are reported as mean \pm SD. $p < 0.05$ was considered statistically significant.

RESULTS

The first dog studied was not imaged with the balloon deflated. In addition, one dog suffered fatal arrhythmias

Figure 1. Representative tagged MR images at end-diastole (left) and end-systole (right) in short-axis view with 0-degree parallel tags (a) and 90-degree parallel tags (b) and in long-axis view (c) in (A) a representative normal dog that did not undergo coronary angiography, (B) a dog before coronary occlusion after coronary angiography and placement of a deflated angioplasty balloon in the LAD coronary artery, and (C) a dog during coronary occlusion by angioplasty balloon inflation. Notice signal void created by inflation of angioplasty balloon with contrast agent (arrow).

Table 1
Maximum Principal Strain

	LAD Bed			LCX Bed		
	Base	Mid	Apex	Base	Mid	Apex
Normal	-0.174 ± 0.03	-0.204 ± 0.03	-0.209 ± 0.04	-0.184 ± 0.03	-0.196 ± 0.03	-0.197 ± 0.04
Baseline	-0.106 ± 0.03*	-0.103 ± 0.03*	-0.112 ± 0.03*	-0.087 ± 0.03*	-0.114 ± 0.03*	-0.121 ± 0.03*

Baseline dogs are dogs with deflated angioplasty balloon in the LAD. Normal dogs are similarly instrumented dogs except no coronary catheterization was performed. Mid is midwall of left ventricle. Values for LAD bed were determined from average of anterior and septal regions for that longitudinal level. Values for LCX bed are the average of posterior and lateral regions for that longitudinal level. Values are means ± SD.

* $p < 0.0001$ vs. same region in normal dogs.

on occlusion and one dog died of anesthetic complications before imaging.

Myocardial Function

Effect of Instrumentation

When maximum contraction (or maximal shortening) at baseline imaging was compared with the 12 identical regions in the normal dogs (e.g., similarly anesthetized and instrumented dogs that had not undergone coronary

catheterization [14]), contraction was globally reduced in both the LAD perfused and left circumflex (LCX) perfused territories of the left ventricle (Table 1). Subtesting revealed a statistically significant reduction in maximum principal strain (or maximal contraction) in all 12 anatomic locations of the instrumented dogs compared with normal dogs ($p < 0.0001$, Scheffé).

It has been previously reported that there is no circumferential variation in maximum contraction in normal dogs (14). There was also no circumferential variation

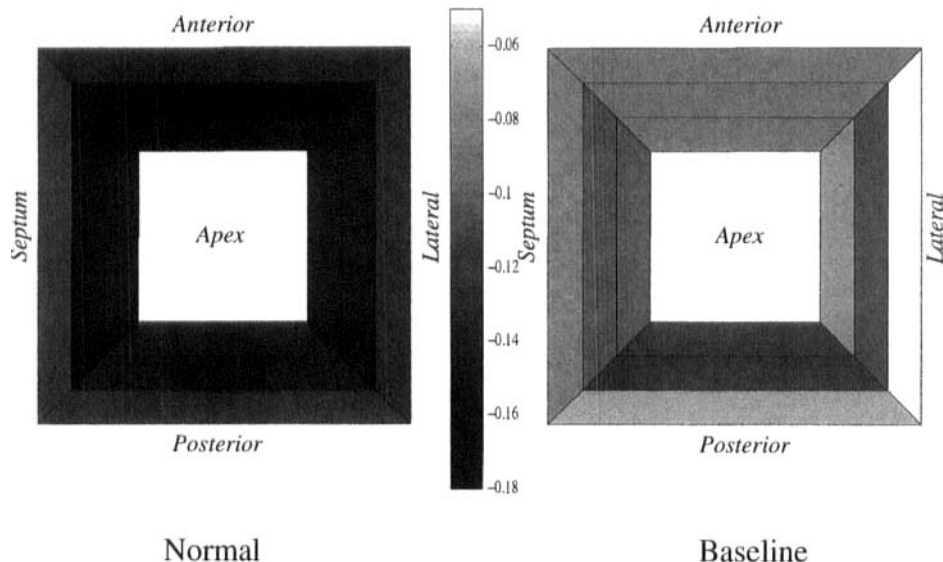


Figure 2. Bulls-eye plots of magnitude of average circumferential strain (or shortening) in normal dogs that did not receive coronary catheterization (left) compared with baseline imaging of dogs after coronary catheterization with deflated angioplasty balloon in LAD (right). Strains were averaged into 12 anatomic regions comprised of three longitudinal levels from base to apex and four circumferential levels (i.e., septum, anterior, lateral, and posterior). Base of heart is toward the outside of the bulls-eye and apex is toward the center. Negative strain represents shortening. Gray scale of shortening goes from white (minimum shortening) to black (maximum shortening). Shortening was reduced in the animals at baseline imaging relative to normal dogs at each of the 12 anatomic regions ($p < 0.001$, Scheffé).

Table 2
Maximum Principal Strain by Transmural Location

	Transmural Location		
	Endocardium	Midwall	Epicardium
Baseline	-0.132 ± 0.04	-0.124 ± 0.03	-0.115 ± 0.03
Occlusion	-0.092 ± 0.04*	-0.089 ± 0.04*	-0.086 ± 0.04†
Early reperfusion	-0.089 ± 0.04*	-0.086 ± 0.04‡	-0.084 ± 0.04†
Late reperfusion	-0.112 ± 0.04	-0.101 ± 0.04	-0.092 ± 0.04

Values are means ± SD. Values for each transmural location (e.g., endocardium) are the average value of five longitudinal (base to apex) and six circumferential regions. * $p < 0.001$ vs. same baseline region by Scheffé subtesting; † $p < 0.04$ vs. same baseline region by Scheffé subtesting; ‡ $p < 0.005$ vs. same baseline region by Scheffé subtesting.

in regional strains in the dogs studied before coronary occlusion (i.e., baseline imaging). However, circumferential shortening with angioplasty instrumentation was reduced at each longitudinal level (i.e., from base to apex) relative to normal dogs (base $p < 0.007$, midventricle $p < 0.015$, and apex $p < 0.003$; Scheffé). By circumferential location, the lateral and anterior walls had significantly reduced shortening at baseline relative to normal dogs (anterior $p < 0.02$ and lateral $p < 0.04$;

Scheffé). Severe reductions in circumferential shortening can be appreciated in a gray-scale representation of the average circumferential shortening by anatomic region shown as bulls-eye plots in Fig. 2 for the group of normal dogs and instrumented dogs at baseline imaging.

Function During Occlusion and Reperfusion

During occlusion, maximum shortening showed a significant reduction from endocardium to epicardium rela-

Table 3
Maximum Principal Strain in Anteroseptal and Anterior Regions

	Anteroseptal			Anterior		
	Endo	Mid	Epi	Endo	Mid	Epi
<i>Mid2</i>						
Baseline	-0.10 ± 0.03	-0.10 ± 0.02	-0.09 ± 0.02	-0.11 ± 0.02	-0.11 ± 0.02	-0.10 ± 0.03
Occlusion	-0.07 ± 0.02*	-0.08 ± 0.02	-0.08 ± 0.03	-0.07 ± 0.02†	-0.07 ± 0.02†	-0.07 ± 0.03*
Early	-0.11 ± 0.02	-0.08 ± 0.01	-0.07 ± 0.01	-0.07 ± 0.04‡	-0.09 ± 0.04	-0.09 ± 0.04
Late	-0.09 ± 0.01	-0.08 ± 0.01	-0.08 ± 0.01	-0.10 ± 0.02	-0.09 ± 0.02	-0.09 ± 0.02
<i>Apex1</i>						
Baseline	-0.14 ± 0.04	-0.13 ± 0.03	-0.12 ± 0.03	-0.13 ± 0.04	-0.11 ± 0.04	-0.10 ± 0.04
Occlusion	-0.07 ± 0.06†	-0.06 ± 0.07†	-0.07 ± 0.06†	-0.06 ± 0.05†	-0.07 ± 0.05†	-0.06 ± 0.04*
Early	-0.07 ± 0.06†	-0.07 ± 0.05†	-0.07 ± 0.04†	-0.07 ± 0.06†	-0.06 ± 0.06†	-0.06 ± 0.03†
Late	-0.10 ± 0.04	-0.10 ± 0.03	-0.09 ± 0.03	-0.11 ± 0.03	-0.10 ± 0.04	-0.10 ± 0.05
<i>Apex2</i>						
Baseline	-0.11 ± 0.04	-0.11 ± 0.03	-0.11 ± 0.03	-0.11 ± 0.02	-0.11 ± 0.02	-0.10 ± 0.02
Occlusion	-0.09 ± 0.05	-0.07 ± 0.05*	-0.08 ± 0.05*	-0.10 ± 0.05	-0.09 ± 0.05	-0.08 ± 0.05
Early	-0.08 ± 0.06§	-0.07 ± 0.06§	-0.07 ± 0.05†	-0.09 ± 0.04	-0.08 ± 0.04‡	-0.07 ± 0.03§
Late	-0.11 ± 0.04	-0.12 ± 0.04	-0.11 ± 0.04	-0.11 ± 0.03	-0.13 ± 0.07	-0.13 ± 0.06

Values are means ± SD.

Endo, endocardial wall; Mid, midventricular wall; Epi, epicardial wall; mid2, apical midventricular slice; apex1, more basal apical slice; apex2, most apical slice.

* $p < 0.02$ vs. same baseline region by Scheffé subtesting; † $p < 0.03$ vs. same baseline region by Scheffé subtesting; § $p < 0.005$ vs. same baseline region by Scheffé subtesting. ‡ $p < 0.0001$ vs. same baseline region by Scheffé subtesting.

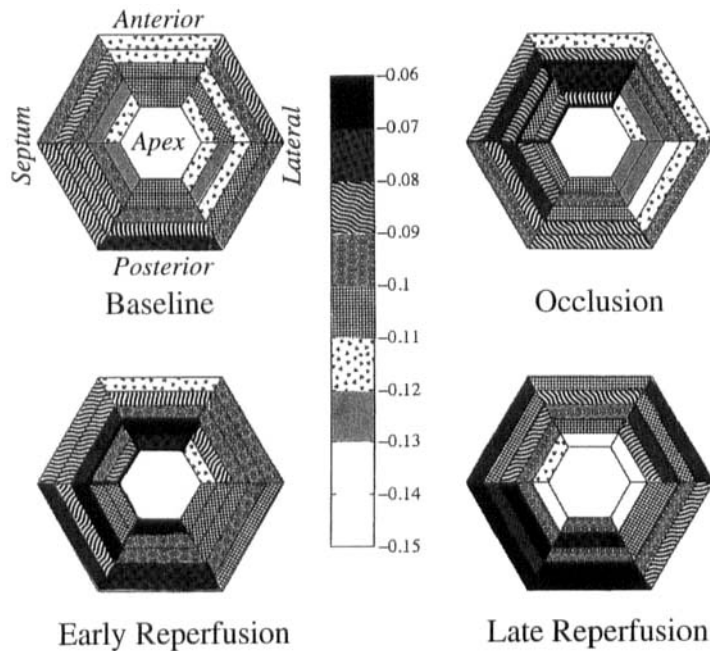


Figure 3. Average maximum principal strain in eight dogs determined from tagged MRI at baseline (top left), during coronary occlusion (top right), after 15 min of reperfusion (bottom left), and after 30 min of reperfusion (bottom right) displayed as bulls-eye plots. Negative strains represent wall shortening. Bulls-eye plots display average strains for midventricular wall; endocardial and epicardial strain values are not shown. Each sector of the bulls-eye plot represents average of strain values for anatomic regions; 30 anatomic regions are shown comprised of five longitudinal levels from base (toward outside of bulls-eye plot) to apex (toward center of bulls-eye plot) and six circumferential locations. Bar in center of graph shows texture map lookup table for strain values. Significant reductions in maximum shortening from baseline are encompassed by bold highlighted regions (i.e., anteroseptal and anterior regions of apex) during occlusion and early reperfusion.

tive to baseline imaging and did not recover during early reperfusion (Table 2). By late reperfusion, maximal shortening had returned to baseline values. Subtesting revealed that this reduction in maximum shortening by transmural location during occlusion and early reperfusion resulted from impaired shortening in the anterior and anteroseptal walls (Table 3) at the midventricular level (mid1) and apical levels (apex1 and apex2). A bulls-eye plot representation of the average maximal shortening restricted to the midwall transmural location (e.g., epicardial and endocardial regions are not shown) demonstrates the regions of reduced maximal shortening from baseline imaging to occlusion to reperfusion (bold lined region, Fig. 3) with the more basilar levels and posterolateral regions remaining functionally unaffected by coronary occlusion and reperfusion.

There was a trend toward reduced circumferential shortening (i.e., circumferential strain) in the LAD bed during occlusion compared with baseline, but a level of statistical significance was not reached by ANOVA. In some animals, dyskinetic motion (i.e., circumferential

stretching rather than circumferential shortening) was observed in the region of the LAD bed during occlusion, whereas other animals had hypokinetic or akinetic motion (i.e., reduced circumferential strain) during LAD occlusion. The variation in circumferential shortening at baseline and during occlusion is demonstrated for two dogs in an apical level (i.e., apex1 level) in Fig. 4. In one dog (dog A), circumferential shortening is more impaired at baseline than in the other dog (dog B). Although circumferential shortening is reduced in both animals during occlusion in the LAD bed, dyskinetic motion is observed in dog A versus hypokinetic motion that is observed in dog B. Thus, a larger interanimal variability (or SD) in circumferential strain prevented the detection of a significant reduction in circumferential shortening in the animals as a group in any circumferential region (Fig. 5) or longitudinal region. Thus, no change in circumferential shortening was observed from baseline to occlusion to reperfusion.

Because of the limited number of tag lines across the ventricular wall, the variance in radial strain at all four

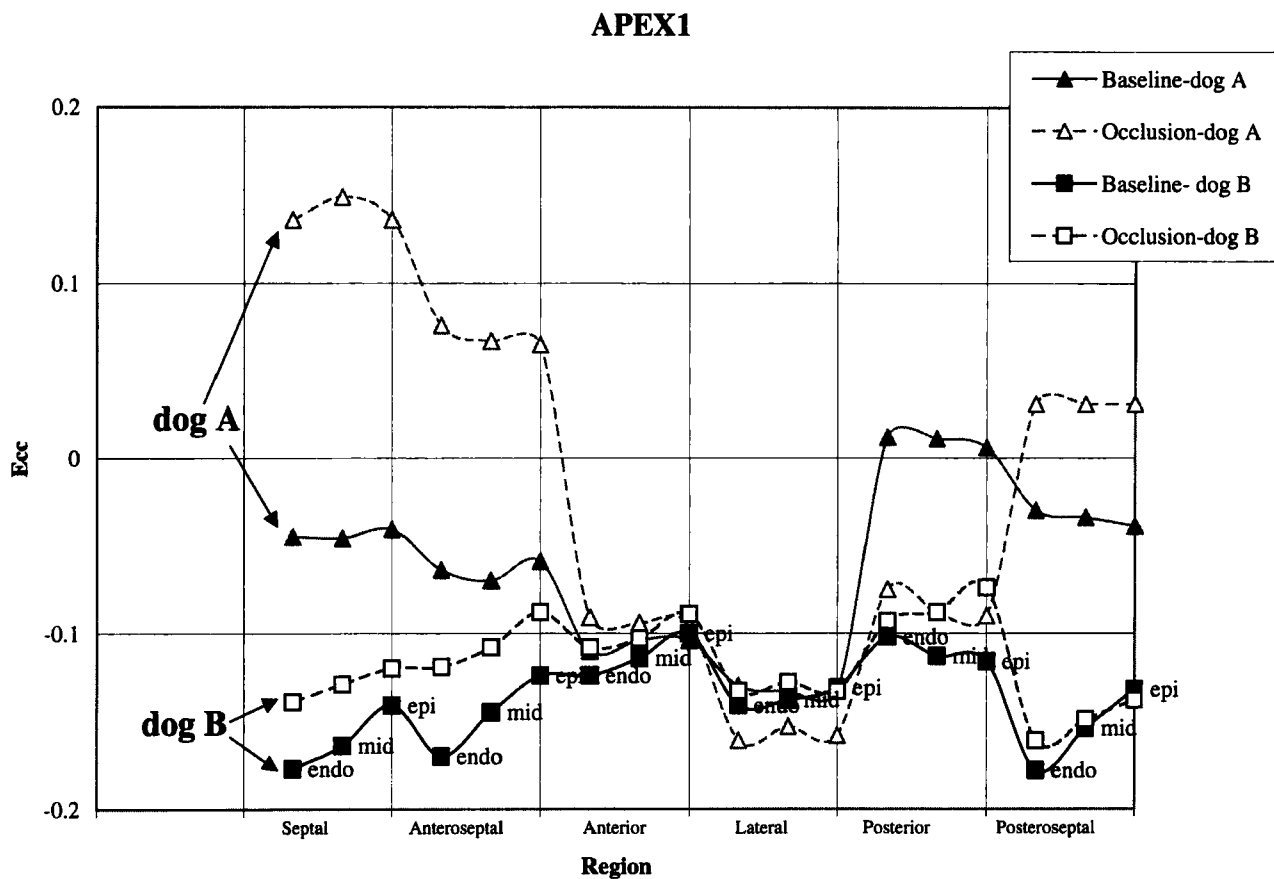


Figure 4. Circumferential shortening in two representative dogs at baseline imaging (e.g., after instrumentation) and during coronary occlusion. Average circumferential strain (Ecc) for each dog was calculated for six circumferential regions at each of three transmural locations in the fourth apical level (APEX1). Increased circumferential shortening is a more negative value with positive values representing circumferential stretching. Dog A had decreased circumferential shortening in the LAD bed (e.g., septal and anteroseptal regions) at baseline imaging compared with dog B. Circumferential stretching (i.e., dyskinetic motion) occurs during occlusion in dog A, whereas reduced circumferential shortening (i.e., hypokinetic motion) occurs during occlusion in dog B.

time points (i.e., baseline, occlusion, early reperfusion, and late reperfusion) was increased relative to the variance in circumferential strain (-0.079 average SD of radial thickening in all regions vs. -0.037 average SD in circumferential shortening in all regions at all times). Thus, no decreased radial thickening was detected during occlusion or early reperfusion relative to baseline in any region.

RMBF and Tissue Viability

Instrumentation Blood Flow

RMBF determined with radiolabeled microspheres showed a significant decline in both the LAD and LCX beds (46% [$p < 0.0009$] and 49% [$p < 0.0003$] reduction, respectively) after the deflated angioplasty balloon

was placed in the LAD compared with the same bed before coronary catheterization. Further diminution in LCX RMBF did not occur with the balloon inflated in the LAD. However, balloon inflation resulted in a significant reduction of 56% on average of RMBF to the LAD bed compared with blood flow with the deflated balloon in place ($p < 0.003$, Scheffé). All three hearts demonstrated completely viable myocardium based on postmortem TTC staining.

Occlusion/Reperfusion Blood Flow and Viability

RMBF determined from fluorescent microspheres in the eight animals demonstrated total absence of flow in the LAD coronary artery bed during angioplasty balloon

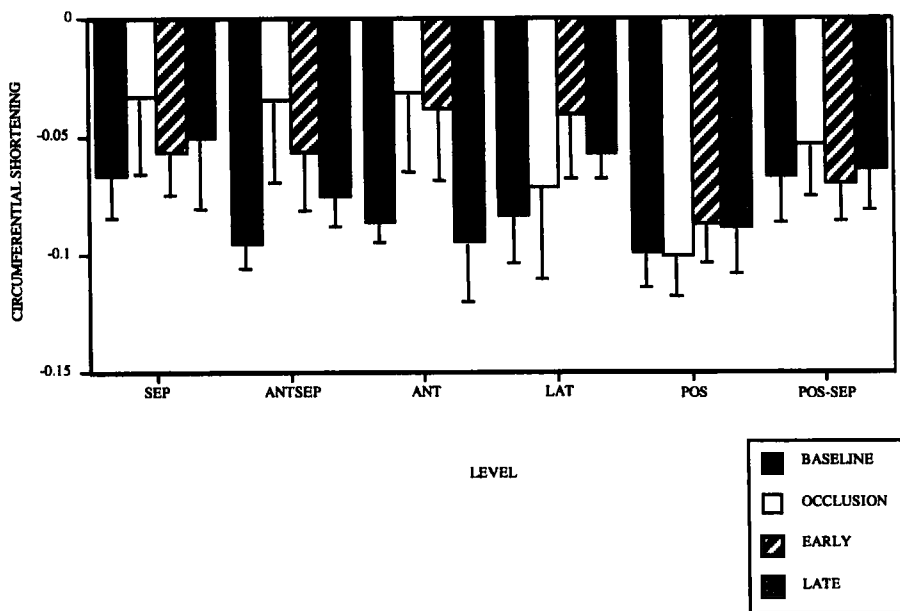


Figure 5. Average circumferential normal strain, where negative strain represents shortening along the circumference of the ventricle, shown by anatomic region (SEP, septum; ANTSEP, anteroseptal; ANT, anterior; LAT, lateral; POS, posterior; POS-SEP, posteroseptal) at four time points (i.e., baseline, occlusion, early reperfusion [EARLY], and late reperfusion [LATE]) in eight dogs subjected to myocardial stunning. Each anatomic region is the average of strain from base to apex. There is a trend toward reduced shortening in the LAD bed (i.e., SEP, ANTSEP, ANT) during occlusion and early reperfusion, whereas the LCX bed (i.e., LAT, POS, POS-SEP) does not show the same decline. A large interanimal variation shown as standard error bars was present such that no statistically significant reduction in circumferential shortening could be detected with coronary occlusion.

inflation. RMBF in the LAD bed after 30 min of reperfusion was not significantly different from LCX RMBF. In the first animal, the deflated angioplasty balloon was not removed during reperfusion; a small area of nonviable myocardium ($<0.45 \text{ cm}^3$) involving the anterior papillary muscle was observed with TTC staining. The protocol was altered on subsequent animals such that the deflated balloon was removed during reperfusion; the remaining animals showed 100% viable myocardium based on TTC staining.

DISCUSSION

Previous studies using open-chest techniques to create coronary occlusion demonstrated consistent abnormalities in contractile function in the ischemic region (3, 18, 19). Thus, the decreased maximum principal strain or maximum shortening after coronary occlusion and early after reperfusion observed in our noninvasive closed-chest model is in agreement with these previous studies.

However, our data comparing baseline function from

this tagged MRI study to previously studied similarly instrumented normal dogs (12) who did not receive coronary catheterization indicated that myocardial function was diminished both regionally and globally secondary to coronary catheterization (and placement of a deflated angioplasty balloon). The 1-mm diameter of the deflated angioplasty balloon would, at best, result in a 30% coronary stenosis in the LAD and minimal stenosis of the left main and LCX coronary artery. Thus, ischemia secondary to instrumentation would not be anticipated.

Nonetheless, detailed radiolabeled microsphere measurements performed in this study documented a 40–50% decline in blood flow in both the LCX and LAD 1 hr after placement of the deflated angioplasty balloon. Thus, it can be inferred that during baseline imaging, blood flow was reduced approximately 40–50% in both the LAD and LCX bed. The observed effect of this decrease in blood flow was a decrease in maximum shortening in every left ventricular region at baseline imaging relative to dogs that did not receive coronary catheterization and angioplasty balloon instrumentation.

Arai et al. (20) showed that gradual reductions in

blood flow over a half hour to achieve a total blood flow decrease of 35% can cause significant reductions in systolic wall thickening without systemic hemodynamic effects or alterations to energy metabolism. Bristow et al. (21) demonstrated a similar consistent relationship between reductions in blood flow during acute ischemia and segmental wall thickening. Gallagher, Ross, and colleagues (22–26) studied this relationship between reductions in mechanical function and blood flow extensively. They showed that a small decrease to subendocardial flow of 18% causes a proportional 13% decrease in systolic wall thickening based on ultrasonic crystal measurements (23). Further diminutions in blood flow led to greater depression in wall thickening. These studies suggest that noncritical stenosis may cause depression of myocardial function with dyskinesia occurring only after severe reductions in blood flow (21,23–25). This concept of a graded response in myocardial function to reductions in blood flow underlies much of the concept of hibernating myocardium (27–29). Although we are not prepared to suggest that the decreased baseline function in our instrumented animals represents hibernating myocardium, the reductions in blood flow due to coronary angiography and deflated balloon placement were not anticipated. Nonetheless, the response of the myocardium at baseline imaging of reduced function is consistent with previous studies of graded responses to reductions in blood flow.

Further reductions in blood flow to the LAD bed during coronary occlusion resulted in diminished myocardial function in the ischemic zone but no change in myocardial function in the nonischemic bed. Heyndrickx et al. (3) showed a variable response in the nonischemic bed with approximately 30% of the dogs exhibiting increased contractility and another approximately 30% exhibiting decreased contractility. Similarly, Buda et al. (30) also observed augmentation in function in the nonischemic regions. However, subsequent studies in closed-chest conscious dogs indicate that this augmentation of function occurs primarily in anesthetized open-chest animal models (31). In our study, radiolabeled microsphere measurements indicated that during balloon LAD angioplasty occlusion, LCX blood flow was not altered. Thus, the observation that mechanical function in the LCX bed is preserved and not augmented during LAD occlusion would suggest that our closed-chest animal model more closely mimics closed-chest conscious ischemia.

Heyndrickx et al. (5) also observed an increased systolic wall thickening during the reactive hyperemia phase of early reperfusion in the stunned myocardium. No rebound in mechanical function occurred in the stunned myocardium in our study. It has been suggested that the reactive hyperemia phase normally subsides 5–10 min

after reperfusion (3,32). Thus, because our first assessment of function was after 15 min of reperfusion, we were unable to confirm whether a rebound in mechanical function occurs. However, we were able to document a progressive improvement in mechanical function in stunned myocardium over the first hour of reperfusion. Although mechanical function in late reperfusion was not significantly different than baseline function, it should be noted that baseline function in our dogs was decreased relative to normal dogs that had not received coronary catheterization. Thus, mechanical function was still depressed after myocardial stunning at 1 hr.

Of particular concern was our inability to document reductions in circumferential shortening and radial thickening during coronary occlusion in the LAD bed in these animals. We believe that the interaction of two factors led to this unexpected result. First, the function at baseline imaging was decreased relative to normal animals. Second, the variance in the strain measurements during occlusion increased relative to baseline imaging in part due to the interanimal variability in the anatomic region affected by occlusion and to the degree of dysfunction caused by short-term coronary occlusion. Typically, in normal anesthetized animals, the variability in normal radial strain is approximately 20% (33). In the present study, the variance in radial and circumferential strain doubled after occlusion and reperfusion.

In particular, we present an example to illustrate how these two factors could interact to prevent the detection of reductions in circumferential shortening and radial thickening with coronary occlusion. Let us compare strain at an anatomic level at which we would anticipate a significant mechanical dysfunction with occlusion in most animals, the fourth longitudinal level (apex1) in the anteroseptal endocardial wall. Mean circumferential shortening (with SD) at baseline imaging in these animals was -0.117 ± 0.032 , whereas during occlusion the average circumferential shortening was -0.043 ± 0.096 . Even if circumferential shortening had ceased with coronary occlusion (e.g., zero shortening), with the same degree of variance in the measure, a statistically significant reduction in circumferential shortening would not have been achieved. However, it is likely that with occlusion some animals may exhibit akinetic motion whereas others may exhibit dyskinetic motion. Therefore, the variance in circumferential shortening is likely to increase during occlusion in this region as occurred in this study. Thus, the ability to demonstrate statistically significant changes to circumferential shortening or radial thickening would be difficult. However, we cannot rule out that by using a larger sample size, a statistically significant change in circumferential shortening and radial

thickening could have been observed during coronary occlusion.

Typically, most quantitative studies of regional one-(1D) and two-dimensional (2D) myocardial function using MR tagging have measured circumferential shortening rather than radial thickening (33–40). The rationale behind using indices of circumferential shortening rather than wall thickening is related to the increased tag density in the circumferential direction relative to the radial direction, leading to improved accuracy in circumferential measurements (33,42). In a recent study, Moore et al. (41) showed that wall thickening and radial strain are the least-sensitive deformation parameters (as compared with longitudinal strain and a shortening index comprised of longitudinal and circumferential strain) for detecting declines in perfusion. Because we have only performed a strain analysis using short-axis images, longitudinal strain measurements were not calculated in this study.

Furthermore, using 1D, 2D, and 3D analysis techniques, it has been demonstrated that the region of myocardial dysfunction is larger than the area of myocardial infarction (14,42,43). This dysfunctional region adjacent to the myocardial infarction would presumably include a combination of viable stunned myocardium and myocardium that has mechanical alterations due to tethering. Thus, as expected in this 2D stunning study, we were able to demonstrate similar dysfunction in stunned tissue based on maximum shortening. However, the severe decline in myocardial function due to coronary angiography and angioplasty balloon instrumentation prevented the detection of dysfunction in other parameters except the parameter with the largest magnitude, maximum principal strain. Ongoing studies of myocardial stunning using MR tagging to circumvent the decline in function due to instrumentation have shown that not only maximum shortening but circumferential shortening are affected in stunning (45). 3D tagging analysis techniques also offer a means to more accurately calculate radial strain (or thickening) from longitudinal and circumferential strain using the assumption of conservation of tissue volume. Croisille et al. (12) recently demonstrated, in a canine model of myocardial infarction, the sensitivity of this radial strain for identifying nonviable tissue. Using this same assumption, we could speculate in our study of stunned animals, based on reductions in maximum shortening, that radial thickening was reduced during coronary occlusion and early reperfusion. Therefore, these tagging techniques may present a noninvasive method to study myocardial dysfunction caused by short ischemic episodes, leading to myocardial stunning and longer ischemic episodes resulting in myocardial infarction.

The observed decline in myocardial function due to angiography and angioplasty balloon placement may have implications in the clinical realm. For example, during angiography, devices that limit coronary perfusion should be rapidly deployed to minimize the likelihood of inducing reversible myocardial dysfunction. In addition, the removal of angioplasty balloons used for enlarging stenotic regions and stenting should also be performed expeditiously to reduce the chances of creation of myocardial infarction, as occurred here in our first animal.

In conclusion, we present here a noninvasive closed-chest technique to create myocardial stunning that produces results similar to those found in closed-chest conscious dogs. Using tagged MRI, myocardial strain in the entire left ventricle was determined noninvasively. Global reductions in myocardial function with concurrent blood flow reductions from coronary catheterization and placement of a deflated angioplasty balloon were documented, as was severe impairment in contraction during occlusion and early reperfusion. Thus, a graded response to myocardial ischemia and short-term dysfunction in viable myocardium after severe ischemia were observed. If baseline function was determined before coronary angiography, the animal model presented here would be well suited for studying myocardial stunning more extensively. In addition, the imaging protocol used in our study, as well as the magnitude of depression of maximum contraction, could be used as benchmarks to determine the extent of myocardial stunning in patients.

ACKNOWLEDGMENTS

Supported by the Heart, Lung, and Blood Institute at the National Institutes of Health (R01-HL45090-08). We thank Anthony DiPaula for assistance with the animal preparation and radiolabeled microsphere measurements and Mary McAllister for editorial assistance.

REFERENCES

1. Kloner R and Braunwald E. Review: observations on experimental myocardial infarction. *Cardiovasc Res* 1980; 14:371–395.
2. Reimer KA and Jennings RB. Pathobiology of acute myocardial ischemia: metabolic, functional, and ultrastructural studies. *Am J Cardiol* 1983; 52:72A–81A.
3. Heyndrickx GR, Millard RW, McRitchie RJ, Maroko PR and Vatner SF. Regional myocardial functional and electrophysiological alterations after brief coronary artery oc-

- clusion in conscious dogs. *J Clin Invest* 1975; 56:978–985.
4. Braunwald E and Kloner RA. The stunned myocardium: prolonged postischemic ventricular dysfunction. *Circulation* 1982; 66:1146–1149.
 5. Heyndrickx G, Wijns W, Vogelaers D, Degrieck Y, Bol A, Vandeplassche G and Melin J. Recovery of regional contractile function and oxidative metabolism in stunned myocardium induced by 1-hour circumflex coronary artery stenosis in chronically instrumented dogs. *Circ Res* 1993; 72:901–913.
 6. Shen YT and Vatner SF. Differences in myocardial stunning following coronary artery occlusion in conscious dogs, pigs, and baboons. *Am J Physiol* 1996; 270:H1312–H1322.
 7. Meza MF, Kates MA, Barbee RW, Revall S, Perry B, Murgo JP and Cheirif J. Combination of dobutamine and myocardial contrast echocardiography to differentiate postischemic from infarcted myocardium. *J Am Coll Cardiol* 1997; 29:974–984.
 8. Vatner SF. Correlation between acute reductions in myocardial blood flow and function in conscious dogs. *Circ Res* 1980; 47:201–207.
 9. Szolar D, Saeed M, Wendland M, Sakuma J, Roberts T, Stiskal M, Derugin N and Higgins C. MR imaging characterization of postischemic myocardial dysfunction ("stunned myocardium"): relationship between functional and perfusion abnormalities. *JMRI* 1996; 6:615–624.
 10. Zerhouni EA, Parish DM, Rogers WJ, Yang A and Shapiro EP. Human heart: tagging with MR imaging—a method for noninvasive assessment of myocardial motion. *Radiology* 1988; 169:59–63.
 11. Axel L and Dougherty L. Heart wall motion: improved method of spatial modulation of magnetization for MR imaging. *Radiology* 1989; 172:349–350.
 12. Croisille P, Moore CC, Judd RM, Lima JAC, Arai M, McVeigh ER, Becker LC and Zerhouni EA. Differentiation of viable and nonviable myocardium by the use of three-dimensional tagged MRI in 2-day-old reperfused canine infarcts. *Circulation* 1999; 99:284–291.
 13. Rochitte CE, Lima JA, Bluemke DA, Reeder SB, McVeigh ER, Furuta T, Becker LC and Melin JA. Magnitude and time course of microvascular obstruction and tissue injury after acute myocardial infarction. *Circulation* 1998; 98:1006–1014.
 14. Kraitchman DL, Young AA, Bloomgarden DC, Fayad ZA, Dougherty L, Ferrari VA and Axel L. Integrated MRI assessment of regional function and perfusion in canine myocardial infarction. *Magn Reson Med* 1998; 40:311–326.
 15. Axel L and Dougherty L. MR imaging of motion with spatial modulation of magnetization. *Radiology* 1989; 171:841–845.
 16. Ambrosio F, Weismann HF, Mannisi JA and Becker LC. Progressive impairment of regional myocardial perfusion after initial restoration of postischemic blood flow. *Circulation* 1989; 80:1846–1861.
 17. Guttman MA, Zerhouni EA and McVeigh ER. Analysis and visualization of cardiac function from MR images. *IEEE Comp Graph Appl* 1997; 17:30–38.
 18. Theroux P, Ross Jr J, Franklin D, Covell JW, Bloor CM and Sasayama S. Regional myocardial function and dimensions early and late after myocardial infarction in the unanesthetized dog. *Circ Res* 1977; 40:158–165.
 19. Ambrosio G, Jacobus W, Mitchell M, Litt M and Becker L. Effects of ATP precursors on ATP and free ADP content and function recovery of postischemic hearts. *Am J Physiol* 1989; 256:H560–H566.
 20. Arai AE, Grauer SE, Anselone CG, Pantely GA and Bristow JD. Metabolic adaptation to a gradual reduction in myocardial blood flow. *Circulation* 1995; 92:244–252.
 21. Bristow JD, Arai AE, Anselone CG and Pantely GA. Response to myocardial ischemia as a regulated process. *Circulation* 1991; 84:2580–2587.
 22. Gallagher K, Kumada T, Koziol J, McKown M, Kemper S and Ross J Jr. Significance of regional wall thickening abnormality relative to transmural myocardial perfusion in anesthetized dogs. *Circulation* 1980; 62:1266–1274.
 23. Gallagher KP, Matsuzaki M, Koziol JA, Kemper WS and Ross J Jr. Regional myocardial perfusion and wall thickening during ischemia in conscious dogs. *Am J Physiol* 1984; 247:H727–H738.
 24. Torry RJ, Myers JH, Adler AL, Liut CL and Gallagher KP. Effects of nontransmural ischemia on inner and outer wall thickening in the canine left ventricle. *Am Heart J* 1991; 122:1292–1299.
 25. Ross J Jr, Gallagher KP, Matzusaki M, Lee JD, Guth B and Goldfarb R. Regional myocardial blood flow and function in experimental myocardial ischemia. *Can J Cardiol* 1986; Jul (Suppl):9A–18A.
 26. Ross J Jr, Gallagher KP, Matzusaki M, Lee JD, Guth B and Goldfarb R. Regional myocardial blood flow and function in experimental myocardial ischemia. *Can J Cardiol* 1986; Jul (Suppl):9A–18A.
 27. Rahimtoola SH. The hibernating myocardium. *Am Heart J* 1989; 117:211–221.
 28. Rahimtoola SH. Hibernating myocardium has reduced blood flow at rest that increases with low-dose dobutamine [editorial; comment] [see comments]. *Circulation* 1996; 94:3055–3061.
 29. Braunwald E and Rutherford JD. Reversible ischemic left ventricular dysfunction: evidence for the "hibernating myocardium." *J Am Coll Cardiol* 1986; 8:1467–1470.
 30. Buda AJ, Lefkowitz CA and Gallagher KP. Augmentation of regional function in nonischemic myocardium during coronary occlusion measured with two-dimensional echocardiography. *J Am Coll Cardiol* 1990; 16:175–180.
 31. Ning X, Zweng T and Gallagher K. Ejection- and isovolumic contraction-phase wall thickening in nonischemic myocardium during coronary occlusion. *Am J Physiol* 1990; 258:H490–H499.
 32. Warltier D, Gross G, Brooks H and Preuss K. Improve-

- ment of postischemic contractile function by calcium channel blocking agent nitrendipine in conscious dogs. *J Cardiovasc Pharmacol* 1988; 1:S120–S124.
- 33. Moore C, McVeigh E and Zerhouni E. Noninvasive measurement of three-dimensional myocardial deformation with tagged magnetic resonance imaging during graded local ischemia. *J Cardiovasc Magn Reson* 1999; 1:207–222.
 - 34. Clark NR, Tallant B, Palmon LC, Yeon SB, Lima JA, Axel L and Reichek N. Noninvasive depiction of stunned myocardium using MRI tagging and magnetite contrast. *Circulation* 1991; 84:II-202.
 - 35. Geskin G, Kramer CM, Rogers WJ, Theobald TM, Pakstis D, Hu YL and Reichek N. Quantitative assessment of myocardial viability after infarction by dobutamine magnetic resonance tagging. *Circulation* 1998; 98: 217–223.
 - 36. Kramer CM, Rogers WJ, Theobald TM, Simonetti O and Reichek N. Remote region dysfunction early after reperfused anterior myocardial infarction: a breath-hold magnetic resonance tissue tagging study. *Circulation* 1994; 90:I-610.
 - 37. Kramer CM, Rogers WJ, Theobald TM, Power TP, Petruolo S and Reichek N. Remote noninfarcted region dysfunction soon after first anterior myocardial infarction. A magnetic resonance tagging study. *Circulation* 1996; 94: 660–666.
 - 38. Lima JA, Jeremy R, Guier W, Bouton S, Zerhouni EA, McVeigh E, Buchalter MB, Weisfeldt ML, Shapiro EP and Weiss JL. Accurate systolic wall thickening by nuclear magnetic resonance imaging with tissue tagging: correlation with sonomicrometers in normal and ischemic myocardium. *J Am Coll Cardiol* 1993; 21:1741–1751.
 - 39. Marcus JT, Gotte MJ, Van Rossum AC, Kuijer JP, Heethaar RM, Axel L and Visser CA. Myocardial function in infarcted and remote regions early after infarction in man: assessment by magnetic resonance tagging and strain analysis. *Magn Reson Med* 1997; 38:803–810.
 - 40. Young AA, Kraitchman DL, Dougherty L and Axel L. Tracking and finite element analysis of stripe deformation in magnetic resonance tagging. *IEEE Trans Med Imag* 1995; 14:413–421.
 - 41. Bazille A, Guttman M, McVeigh E and Zerhouni E. Impact of semiautomated versus manual image segmentation errors on myocardial strain calculation by magnetic resonance tagging. *Invest Radiol* 1994; 29:427–433.
 - 42. Kramer CM, Lima JA, Reichek N, et al. Regional differences in function within noninfarcted myocardium during left ventricular remodeling. *Circulation* 1993; 88:1279–1288.
 - 43. Kramer CM, Rogers WJ, Theobald TM, Power TR and Reichek N. Left ventricular dilatation progresses despite resolution of remote region dysfunction 6 months after anterior myocardial infarction. *Circulation* 1995; 92:I-316.
 - 44. Ozanur I, McVeigh E, Wyman B, Lima J, Bluemke D and Kraitchman D. Detection of viable myocardium with MRI after ischemic injury. *Circulation* 1998; 98:I-857.